Vol. 25, No. 2(2026) Mat26762

Revista Mexicana de Ingeniería Química

A kinetic study on the influence of temperature on cobalt electrodeposition onto a monocrystalline Au(111) electrode

Estudio cinético de la influencia de la temperatura en la electrodeposición de cobalto sobre un electrodo monocristalino de Au(111)

L.H. Mendoza-Huizar*, C.H. Rios-Reyes

Área Académica de Química, Universidad Autónoma del Estado de Hidalgo, carretera Pachuca–Tulancingo, 42184, Mineral de la Reforma, Hidalgo. México.

Received: January 17, 2026; Accepted: March 23, 2026

Abstract

In this work, a kinetic study of cobalt electrodeposition onto Au(111) was carried out from a solution containing 0.005 M $CoCl_2$ in 1 M NH_4Cl (pH 9.5), by means of cyclic voltammetry and potential step methods to assess the influence of temperature. An increase in temperature led to higher kinetic and nucleation parameters, facilitating cobalt reduction onto the Au(111) surface. Nondimensional plots of the current-time transients revealed that the overpotential deposition followed a three-dimensional progressive nucleation model. Analysis of the transients obtained at various applied potentials enabled the determination of the nucleation rate constant and the density of active nucleation sites, both of which increased with more cathodic potentials and elevated temperatures. The temperature dependence of the nucleation and diffusion processes was satisfactorily described by an Arrhenius-type relationship. Apparent activation energies ranging from 24 to 42 kJ·mol^{-1} were calculated for nucleation, while a value of 32.6 kJ·mol^{-1} was obtained for diffusion, indicating that at low overpotentials, cobalt electrodeposition is mainly governed by interfacial nucleation and growth phenomena.

Keywords: kinetic, cobalt, electrodeposition, Au(111), activation energy.

Resumen

En este trabajo, se llevó a cabo un estudio cinético de la electrodeposición de cobalto sobre Au(111) a partir de una solución que contenía 0.005 M $CoCl_2$ en 1 M NH_4Cl (pH 9.5), mediante voltametría cíclica y métodos de escalón de potencial, con el fin de evaluar la influencia de la temperatura. El aumento de la temperatura condujo a valores mayores de los parámetros cinéticos y de nucleación, facilitando la reducción de cobalto en la superficie de Au(111). El trazado adimensional de los transitorios de corriente-tiempo reveló que la deposición por sobrepotencial seguía un modelo de nucleación progresiva tridimensional. El análisis de los transitorios obtenidos a distintos potenciales aplicados permitió determinar la constante de velocidad de nucleación y la densidad de sitios activos de nucleación, ambos incrementándose a potenciales más catódicos y a temperaturas elevadas. La dependencia de la temperatura de los procesos de nucleación y difusión se describió satisfactoriamente mediante un comportamiento tipo Arrhenius. Se calcularon energías de activación aparentes que oscilaron entre 24 y 42 kJ·mol^{-1} para la nucleación, mientras que para la difusión se obtuvo un valor de 32.6 kJ·mol^{-1}, lo que indica que, a bajos sobrepotenciales, la electrodeposición de cobalto está principalmente influenciada por fenómenos de nucleación y crecimiento en la interfaz.

Palabras clave: cinética, cobalto, electrodeposición, Au(111), energía de activación.

*Corresponding author. *E-mail*: hhuizar@uaeh.edu.mx ;
https://doi.org/10.24275/rmiq/Mat26762
ISSN:1665-2738, *issn-e*: 2395-8472

1 Introduction

Cobalt electrodeposits on gold substrates are of particular interest due to the strong perpendicular magnetic anisotropy that arises at the Co/Au interface, enabling potential applications in magnetically functional coatings and nanoscale magnetic systems (Szmaja *et al*., 2012). This interfacial effect has motivated significant scientific attention, as understanding and controlling the growth mechanisms, structural properties, and magnetic behavior of cobalt layers is essential for optimizing their performance in such applications (Chen, Wang, Pradel, Ribes, & Record, 2014; de Abril, Mandler, & Unwin, 2004; Graciano, Bertocci, & Stafford, 2019; Hamulić, Milošev, & Lützenkirchen-Hecht, 2018; Krause, Uhlemann, Gebert, & Schultz, 2004; Lin, Yan, Wang, Fu, & Mao, 2006; Mendoza-Huizar, Robles, & Palomar-Pardavé, 2003; Mendoza-Huizar, Robles, & Palomar-Pardavé, 2002; Wu, Zei, & Yau, 2010). Consequently, cobalt electrodeposition on gold substrates has been extensively investigated in the literature, addressing aspects ranging from electrochemical kinetics and morphology evolution to magnetic and crystallographic properties (Allongue, Cagnon, Gomes, Gündel, & Costa, 2004; Bubendorff, Beaurepaire, Mény, & Bucher, 1998; Chen *et al*., 2014; Cruz-Martínez, Rivera-Hernández, Álvarez-Romero, Nieto-Velázquez, & Mendoza-Huizar, 2021; de Abril *et al*., 2004; Flis-kabulska, 2006; Graciano *et al*., 2019; Hamulić *et al*., 2018; Krause *et al*., 2004; Landa-Castro, Sebastián, Giannotti, Serrà, & Gómez, 2020; Lin *et al*., 2006; Mendoza-Huizar & Rios-Reyes, 2013; Mendoza-Huizar, Robles, & Palomar-Pardave, 2005; Mendoza-Huizar *et al*., 2003; Mendoza-Huizar *et al*., 2002; Szmaja *et al*., 2012; Wu *et al*., 2010).

Cobalt can be electrodeposited onto gold substrates under both underpotential deposition (UPD) (Allongue *et al*., 2004; Cagnon *et al*., 2000; Chen *et al*., 2014; Flis-kabulska, 2006; Marsh *et al*., 2013; Mendoza-Huizar *et al*., 2002) and overpotential deposition (OPD) conditions (Allongue *et al*., 2004; Chen *et al*., 2014; Flis-kabulska, 2006; Mech, Zabiński, Kowalik, & Fitzner, 2012; Mendoza-Huizar *et al*., 2003). During the initial stages of UPD, cobalt deposition often proceeds through the formation of a monolayer governed by combined adsorption and two-dimensional nucleation processes, frequently under diffusion control (Mendoza-Huizar *et al*., 2002). In some cases, a transition from 2D to 3D growth is observed as the applied overpotential increases (L. H. Mendoza-Huizar *et al*., 2005, 2003). Under OPD conditions, the morphology and electrochemical behavior of cobalt deposits are strongly influenced by the composition of the electrodeposition bath and experimental parameters such as pH, applied potential, temperature, and the presence of magnetic fields, or complexing agents. Since these factors affect reduction kinetics and the density of active nucleation sites on the substrate (Armyanov, 2000; Cortés *et al*., 2011; Hamulić *et al*., 2018; Hsieh, Lai, Huang, & Sun, 2014; Kołodziejczyk *et al*., 2018; Wei *et al*., 2009), precise control of these parameters is essential for tailoring structural and functional characteristics of the deposits. Cobalt electrodeposition on gold has been done mainly from electrolytes containing sulfates (Di, Damian, Maroun, & Allongue, 2016; Flis-kabulska, 2006; Graciano *et al*., 2019; Hamulić *et al*., 2018; Krause *et al*., 2004; Montes-Rojas, Torres-Rodríguez, & Nieto-Delgado, 2007; Nemtoi, Chiriac, Dragos, Apostu, & Lutic, 2009; W. Szmaja *et al*., 2012), chlorides (Chen *et al*., 2014; Cruz-Martínez *et al*., 2021; Lützenkirchen-Hecht, Hamulić, Wagner, & Milošev, 2020; Mendoza-Huizar & Rios-Reyes, 2013), nitrates (Hamulić *et al*., 2018), perchlorates (Fayette, Bertocci, & Stafford, 2016), ionic liquids (Lin *et al*., 2006), and deep eutectic solvents (Landa-Castro *et al*., 2020), all of which markedly influence deposition kinetics and film architecture (Allongue *et al*., 2004) Additionally, the presence of different ionic species in solution can modify the surface structure and atomic ordering of the deposits, thereby influencing their final electrical and magnetic properties (García-Torres, Gómez, & Vallés, 2009; Hamulić *et al*., 2018; Krause *et al*., 2004). Futhermore, previous studies have demonstrated that cobalt nucleation on gold is strongly dependent on the crystallographic orientation of the gold substrate as well as on the electrochemical conditions employed (Flis-kabulska, 2006; Mendoza-Huizar *et al*., 2005).

Electrodeposition is affected by several critical variables, such as temperature, which plays a decisive role by directly influencing ionic mobility, charge-transfer rates, and diffusion coefficients. These factors dictate how metal ions behave, impacting both nucleation rates and the growth of nuclei on the electrode surface (Costa, Portela, & de Almeida Neto, 2020; Paunovic & Schlesinger, 2006). Current research highlights that increasing the temperature generally enhances reduction kinetics and modifies charge-transfer coefficients, leading to changes in metal layer formation (Costa *et al*., 2020; Gamburg & Zangari, 2011; Paunovic & Schlesinger, 2006). Despite the continued interest in cobalt electrodeposition and the recognized importance of parameters such as pH and electrolyte composition, the effect of temperature on the nucleation and growth dynamics of cobalt on well-defined crystalline gold surfaces, such as Au(111), remains insufficiently explored (Di *et al*., 2016; Fayette *et al*., 2016; Flis-kabulska, 2006; Lin *et al*., 2006; Mendoza-Huizar *et al*., 2005; Montes-Rojas *et al*., 2007). This is

particularly true for quantitative kinetic models that integrate UPD, OPD, and mass transport effects over a range of temperatures. Accordingly, in this work, the electrodeposition of cobalt on Au(111) is investigated using cyclic voltammetry and potential step techniques to gain a deeper insight into the kinetic processes governing cobalt layer formation. The study focuses on diffusion-controlled deposition under both underpotential and overpotential conditions, as well as on the influence of temperature on these mechanisms.

2 Methodology

Cobalt electrodeposition onto a monocrystalline Au(111) electrode, was carried out from an aqueous electrolyte containing 0.005 M $CoCl_2$ and 1 M NH_4Cl, adjusted to pH 9.5 using NaOH. Experiments were performed at temperatures of 298.15, 303.15, 308.15, and 313.15 K. All solutions were prepared with analytical-grade reagents and ultrapure water (Millipore-Q system, 18.2Ω cm) and were deaerated by nitrogen bubbling for 15 min prior to each experiment. The working electrode consisted of a commercial Au(111) single-crystal substrate (Arrandee^{TM}) with an exposed geometric area of 1.21 cm^2. A graphite rod served as the counter electrode, while an Ag/AgCl (sat. KCl) electrode, connected via a Luggin capillary, was employed as the reference electrode. All measurements were conducted in unstirred solutions. Electrochemical experiments were performed using a BAS potentiostat controlled by BAS100W software. The electrochemical response of the Au(111) electrode in the deposition bath was first evaluated by cyclic voltammetry within a potential range from 0.400 to -1.100 V at scan rates between 10 and 200 mV s^{-1}. Cobalt nucleation kinetics were investigated under potentiostatic conditions by analyzing the current-time (*j-t*) transients obtained via the potential step technique. In all experiments, the initial potential was fixed at 0.400 V, and potential steps ranging -0.86 to -0.96 V were applied in 10 mV increments for 32 s. The electrolyte temperature was maintained using a Techne Tempette TE-8D controller.

3 Results and discussion

3.1 Pourbaix diagram

To identify the chemical species present and evaluate the equilibrium potentials of the system, a thermodynamic analysis was performed using multicomponent Pourbaix diagrams (Rojas-Hernández, Ramírez, Ibáñez, & González, 1991). Cobalt(II) speciation was determined using the Hydra–Medusa software with stability constants obtained from the literature (Dean, J, 1999; Martell & Smith, 1976). Under the experimental conditions (0.005 M $CoCl_2$, 1 M NH_4Cl, pH 9.5), the free ammonia concentration favors the formation of the pentaammine complex $[Co(NH_3)_5]^{2+}$, which constitutes the predominant species in solution. Consequently, the relevant electrochemical process corresponds to the reduction of this complex, described by the half-reaction in equation (1):

$$Co(NH_3)_5^{2+} + 2e \leftrightarrow Co + 5NH_3 \tag{1}$$

Due to strong complexation, the total analytical cobalt concentration cannot be directly used in the Nernst equation. The system must, therefore, be described in terms of a conditional potential (E^0), which accounts for the overall stability constant (β_5) of the $[Co(NH_3)_5]^{2+}$ complex.

$$E' = E_{Co^{2+}/Co^0} - \frac{RT}{2F}\ln\left(a_{Co^{2+}}\right) \tag{2}$$

Activity coefficients were not explicitly considered; therefore, activities were approximated by concentrations, $a_{Co^{2+}} \approx \left[Co^{2+}\right]$, where the concentration of the free Co^{2+} ion is determined by equation (3):

$$\left[Co^{2+}\right] = \frac{C_{Co,total}}{1 + \sum \beta_n [NH_3]^n} \tag{3}$$

The high formation constant significantly decreases the concentration of the free ion, shifting the equilibrium potential toward more negative values. This shift arises from the logarithmic term in the Nernst equation associated with complexation. Under the studied conditions, this shift is -0.216 V relative to the aqueous Co^{2+}/Co^0 couple. Considering that the standard potential of the Co^{2+}/Co^0 system is -0.28 V vs SHE, the effect of complexation leads to a conditional potential of -0.496 V vs SHE. Accounting for the conversion factor of -0.197 V for the Ag/AgCl (sat. KCl) electrode, the conditional potential is equivalent to -0.693 V vs. Ag/AgCl. This result is directly reflected in the multicomponent Pourbaix diagram (Fig. 1), constructed using the algorithm implemented in Hydra-Medusa software (Puigdomenech, 2004), where at pH 9.5, the equilibrium boundary between $[Co(NH_3)_5]^{2+}$ and Co^0 is located precisely at -0.693 V vs Ag/AgCl. The agreement between the calculated value and the equilibrium line in the diagram confirms that the shift toward more negative potentials arises from the thermodynamic stabilization of the cation by the ammonia coordination sphere.

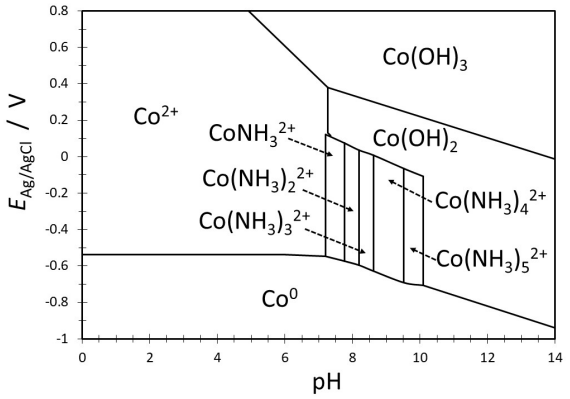

Fig. 1. Pourbaix-type diagram of the Co(II)/Co^0 systems at pCo(II)' '=2.3 and pNH3'=0.0.

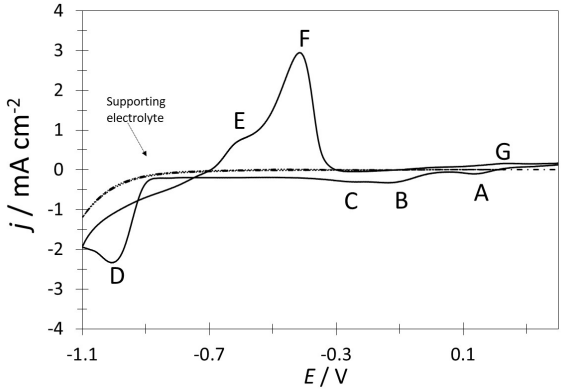

Fig. 2. Cyclic voltammograms of the Au(111)/0.005 M $CoCl_2$ + 1 M NH_4Cl (pH 9.5) and Au(111)/1 M NH_4Cl (pH 9.5) systems at 298.15 K. The potential scan was initiated at 0.400 V and swept in the negative direction to -1.1 V at a scan rate of 20 mV s^{-1}.

3.2 Voltammetric study

Figure 2 presents a cyclic voltammogram recorded for the Au(111)/0.005 M $CoCl_2$ system in 1 M NH_4Cl at pH 9.5 and 298 K (solid line). During the cathodic scan, four distinct current peaks, labeled A, B, C, and D, are observed at approximately 0.140, -0.12, -0.26, and -1.00 V, respectively. To confirm that these signals originate from cobalt deposition, a control voltammetric experiment was performed using the Au(111) electrode in an electrolyte containing only NH_4Cl. Figure 2 also includes a comparison between voltammograms recorded in the presence and absence of Co(II) ions. The absence of these electrochemical signals in the cobalt-free solution demonstrates that peaks A–D are directly associated with cobalt electrodeposition. Under the experimental conditions employed, the dominant cobalt species in solution is the $[Co(NH_3)_5]^{2+}$ complex, and the conditional equilibrium potential of the $[Co(NH_3)_5]^{2+}/Co^0$ redox couple is -0.693 V vs. Ag/AgCl at 298.15 K. This potential value is provided as a reference to indicate the potential region where bulk cobalt deposition becomes thermodynamically favorable and to delineate the boundaries between UPD and OPD regimes. Accordingly, peaks A, B, and C, which appear at potentials more positive than this equilibrium potential for bulk cobalt deposition, are attributed to UPD. In this region, cobalt adatoms are stabilized by strong metal–substrate interactions with the Au(111) surface, enabling deposition at potentials more positive than the Nernst potential for bulk Co. In contrast, peak D, located at significantly more negative potentials (≈ -1.00 V), corresponds to OPD, where three-dimensional nucleation and growth of bulk cobalt occur. Thus, peaks A–D are governed not only by thermodynamic considerations but also by kinetic and interfacial factors, including electron-transfer kinetics, surface diffusion of adatoms, nucleation mechanisms, and possible structural transitions within the cobalt adlayer. The multiplicity of UPD peaks (A–C) suggests the formation of different surface phases or coverage-dependent structural rearrangements prior to the onset of bulk cobalt growth. During the anodic scan, three oxidation peaks, labeled E, F, and G, are observed at approximately -0.620, -0.410, and 0.240 V, respectively. These peaks are assigned to the electrochemical dissolution of the cobalt previously deposited during the cathodic scan. Specifically, the anodic peaks at more negative potentials are typically associated with the dissolution of the bulk deposit (OPD), while those at more positive potentials correspond to the stripping of the UPD layers.

Analysis of the cyclic voltammograms recorded at 298.15 K and at different inversion potentials (Figure 3) reveals a clear correlation between anodic peaks E and F and the dissolution of the cobalt deposited at peak D. These oxidation peaks appear exclusively when the cathodic scan is extended to potentials more negative than -1.0 V, where overpotential deposition of bulk cobalt occurs. Their relatively negative stripping potentials are indicative of the dissolution of three-dimensional cobalt deposits that interact more weakly with the Au(111) surface compared to the UPD layers. In contrast, peak G is observed even when the inversion potential is limited to the underpotential deposition region, where cobalt deposition is restricted to the submonolayer coverage associated with peaks A–C. The more positive potential of peak G reflects the higher thermodynamic stability of cobalt atoms deposited under UPD conditions, which are strongly bound to the gold substrate through strong Co–Au interactions. This behavior is characteristic of UPD systems and is consistent with reports for other transition metals on noble metal surfaces, where the stripping of UPD layers occurs at significantly more positive potentials than that of bulk metal deposits (Bockris, Reddy, & Gamboa-Aldeco, 2002). Accordingly, the correlation between the inversion potential and the position of the dissolution peaks confirms the presence of at least two distinct cobalt

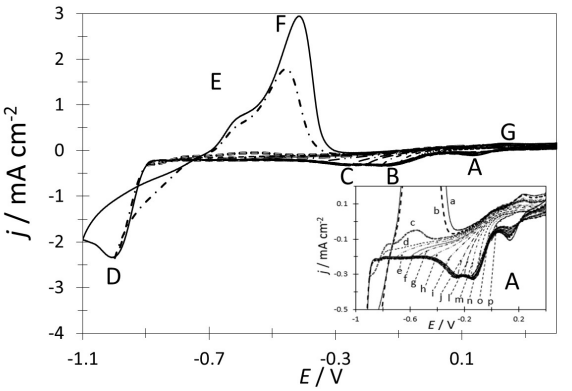

Fig. 3. Cyclic voltammograms obtained in the system Au(111)/0.005 M $CoCl_2$ + 1 M NH_4Cl (pH 9.5) at 298.15 K and at different inversion potentials. In all cases, the potential scan started at 0.400 V towards the negative direction with a potential scan rate of 20 mV s^{-1}. Cathodic and anodic density peak currents are indicated.

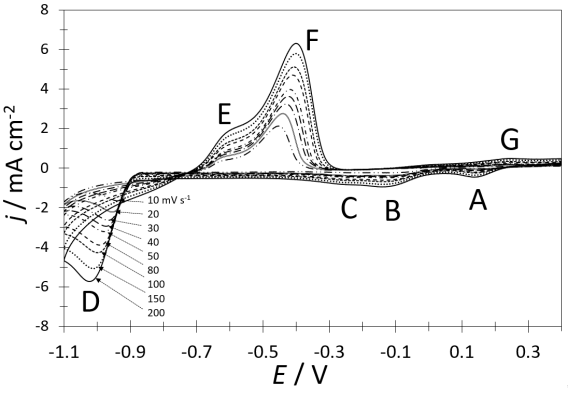

Fig. 4. Cyclic voltammograms recorded from the Au(111)/0.005 M $CoCl_2$ + 1 M NH_4Cl (pH 9.5) system at 298.15 K and different scan rates as is indicated in the figure. In all cases, the potential rate started at 0.400 V towards the negative direction with a potential scan rate of 20 mV s^{-1}.

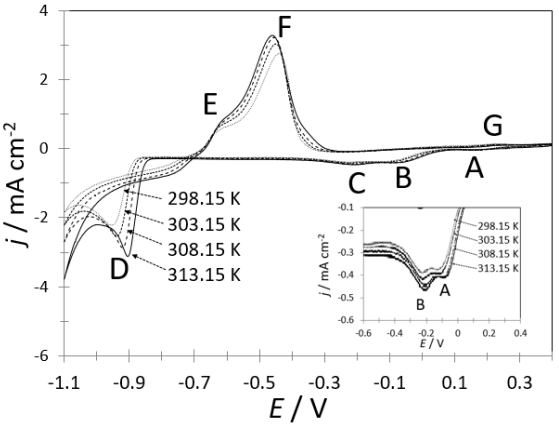

Fig. 5. Typical cyclic voltammogram plots obtained from the Au(111)/0.005 M $CoCl_2$ + 1 M NH_4Cl (pH 9.5) at different temperatures as is indicated in the figure. In all cases, the potential rate started at 0.400 V towards the negative direction with a potential scan rate of 20 mV s^{-1}.

phases on Au(111): a strongly adsorbed UPD layer and a bulk-like OPD deposit, each exhibiting a characteristic anodic response.

Figure 4 shows a set of cyclic voltammograms recorded for the Au(111)/0.005 M $CoCl_2$ system in 1 M NH_4Cl at pH 9.5 and 298.15 K at different potential scan rates. During the cathodic scan, the same reduction peaks previously identified in Fig. 2 are observed. The peak potentials corresponding to A, B, and C remain essentially invariant with increasing scan rate, indicating that these processes exhibit the quasi-equilibrium surface-controlled behavior characteristic of cobalt underpotential deposition (UPD) on Au(111), rather than being strictly thermodynamically controlled. In contrast, peak D shifts systematically toward more negative potentials as the scan rate increases, suggesting that cobalt deposition under overpotential conditions is governed by kinetic limitations and mass transport. The increasing cathodic overpotential reflects a higher energetic barrier for the nucleation and growth of bulk cobalt at faster potential scans, consistent with a three-dimensional (3D) growth mechanism. During the anodic scan, peak E appears at a nearly constant potential over the range of scan rates examined, indicating a comparatively reversible dissolution process associated with a well-defined cobalt phase. By contrast, peaks F and G exhibit progressive shifts toward more positive potentials with increasing scan rate. This behavior is consistent with kinetic polarization effects associated with the stripping of the cobalt deposits. At higher scan rates, a larger overpotential is required to sustain the dissolution current, leading to the observed anodic shift. The dependence of these anodic features on scan rate supports their assignment to the oxidation of cobalt deposits formed under kinetically influenced, quasi-reversible conditions, rather than to changes in the thermodynamic stability of the deposits.

The effect of temperature on the voltammetric peak potentials is shown in Figure 5. An overall increase in current density is observed as temperature increases, which can be attributed to enhanced ionic mobility in the electrode/electrolyte and faster charge-transfer kinetics at the electrode–electrolyte interface (Costa *et al*., 2020; Gamburg & Zangari, 2011; Paunovic & Schlesinger, 2006). The peak potentials associated with the UPD processes (peaks A, B, and C) remain essentially constant over the investigated temperature range. This temperature invariance is consistent with fast interfacial electron-transfer kinetics and surface-limited deposition occurring under quasi-equilibrium conditions, driven by strong Co–Au interactions. Under these circumstances, the peak positions exhibit only minor sensitivity

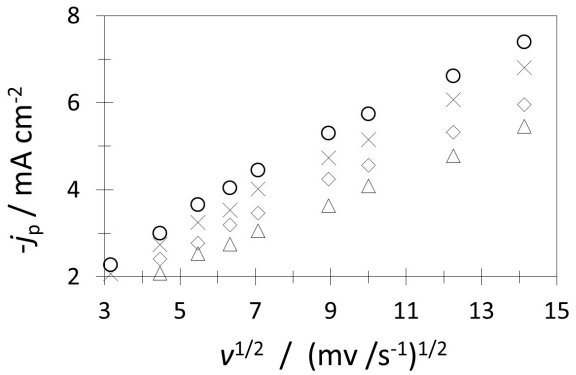

Fig. 6. Plot of the experimental cathodic peak current density D (j_p) as a function of scan rate ($v^{1/2}$) for different temperatures.

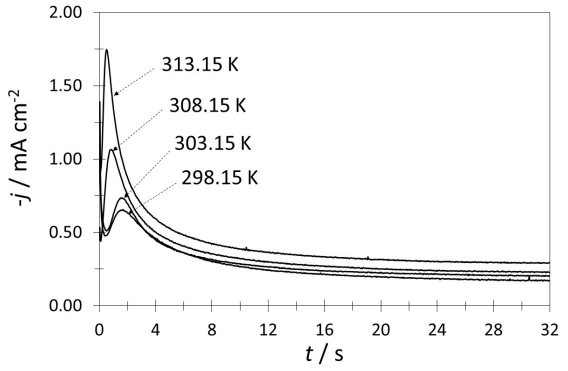

Fig. 7. Experimental current transients recorded from the Au(111)/0.005 M $CoCl_2$ + 1 M NH_4Cl (pH 9.5) system at -0.960 V. In all cases, a starting potential of 0.600 V was applied to the Au(111) electrode surface.

to temperature variations. In contrast, the potential corresponding to peak D shifts systematically toward more positive values with increasing temperature. This behavior indicates that cobalt deposition in the OPD region is thermally activated (Black, Zhang, Noori, Reid, & Bartlett, 2023; Motobayashi, Nakagawa, Shibamura, & Ikeda, 2023). The positive shift reflects accelerated charge-transfer kinetics and a reduced activation barrier for the nucleation and growth of bulk cobalt at elevated temperatures (Motobayashi *et al*., 2023). Therefore, the OPD process is predominantly governed by kinetic factors associated with the activation energy and three-dimensional growth dynamics.

To elucidate the controlling mechanism of cobalt electrodeposition associated with peak D, the peak current density (j_p) was plotted as a function of the square root of the potential scan rate ($v^{1/2}$) according to the Berzins–Delahay equation (Berzins & Delahay, 1953):

$$j_p = 0.6105\left(\frac{F^3}{RT}\right)^{\frac{1}{2}} n^{\frac{3}{2}} D^{\frac{1}{2}} C_0 v^{\frac{1}{2}} \qquad (4)$$

where j_p is the peak current density (in A cm^{-2}), n is the number of electrons transferred, C_0 is the bulk cobalt concentration (mol·cm^{-3}), D is the diffusion coefficient (cm^2·s^{-1}), and v is the scan rate (V·s^{-1}). A linear relationship between j_p and $v^{1/2}$ was observed across all scan rates examined (Figure 6), indicating that the deposition of cobalt under these conditions is a diffusion-controlled process, governed by the transport of cobalt species from the bulk solution to the electrode surface (Berzins & Delahay, 1953).

3.3 Potentiostatic study

Current-time density transients obtained via chronoamperometry provide critical insight into the kinetics of nucleation and growth during electrodeposition. In this study, the technique was applied to determine the kinetic parameters of cobalt electrodeposition on Au(111) at pH 9.5 across a range of temperatures. Figure 7 presents a series of current density transients recorded under OPD conditions (at -0.960 V) using the potential-step method, where the applied potential was held constant while varying only the temperature. Initially, the Au(111) electrode was polarized at 0.400 V, a potential at which cobalt reduction does not occur, ensuring well-defined and reproducible initial conditions. Additionally, current density transients were recorded by applying negative potential steps in the range of -0.860 to -0.960 V. This range was selected based on the prior voltammetric analysis, covering potentials from the onset of cobalt reduction under overpotential conditions to the region of the cathodic current peak. As shown in Figure 7, all current transients (j vs. t) exhibit an initial sharp decay, commonly attributed to the discharge of the electrical double layer and, in some cases, to instantaneous two-dimensional nucleation. This stage is followed by a rise in current to a maximum value (j_m), at a characteristic time (t_m), after which the current gradually decreases toward a diffusion-limited regime. Such behavior is characteristic of three-dimensional nucleation and growth under mass-transfer control (Scharifker & Hills, 1983). The consistent presence of a current maximum, along with the subsequent time-dependent decay typical of diffusion-controlled processes, indicates that cobalt electrodeposition on Au(111) is predominantly governed by the transport of electroactive species from the bulk solution to the electrode surface (Scharifker & Hills, 1983). These observations align with the voltammetric data and reinforce the conclusion that the electrodeposition process proceeds under diffusion-controlled conditions.

Based on the current density transients shown in Figure 7, the nucleation mechanism was analyzed using the Scharifker–Hills model (Scharifker & Hills, 1983). For this purpose, the experimental transients were normalized and represented in a non-dimensional

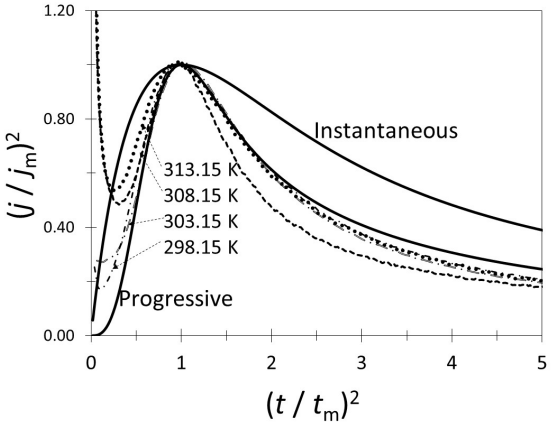

Fig. 8. Comparison of experimental transients normalized (through the coordinates of its respective local maximum (t_m, j_m), with the theoretical nondimensional curves corresponding to 3D instantaneous nucleation (Eq. (5)) and 3D progressive nucleation (Eq. (6)).

form as $j^2/j_m{}^2$ versus t/t_m and compared with the theoretical curves for instantaneous and progressive nucleation described by equations. (5) and (6), respectively (Figure 8). The comparison indicates that, across all applied potentials and temperatures, the electrodeposition of cobalt on Au(111) follows a progressive nucleation mechanism.

$$\frac{j}{j_m^2} = 1.9542\left(\frac{t}{t_m}\right)^{-1}\left\{1-\exp\left[-1.2564\frac{t}{t_m}\right]\right\}^2 \quad (5)$$

$$\frac{j^2}{j_m^2} = 1.2254\left(\frac{t}{t_m}\right)^{-1}\left\{1-\exp\left[-2.3367\left(\frac{t}{t_m}\right)^2\right]\right\}^2 \quad (6)$$

Here, it is important to note that the current decay observed in the transients reported in Figure 7 cannot be adequately explained solely by the double-layer charging process. The incorporation of a 2D instantaneous nucleation (2D-i) model is necessary, taking into account the formation of a monolayer in the UPD region. Further details regarding the equations and the applicability of the model are provided in the Supplementary Material. Accordingly, it has been reported in the literature that transients such as those shown in Figure 7 can be predicted using the following equation (Mendoza-Huizar *et al*., 2002):

$$j(t) = j_{2D-i} + j_{dl} + j_{3D-dc} \quad (7)$$

where the instantaneous 2D nucleation current is given by (Armstrong & Harrison, 1969):

$$j_{2D-i} = k_1 \exp(-k_2 t) \quad (8)$$

the charge of the double layer is represented by:

$$j_{dl} = k_3 \exp(-k_4 t) \quad (9)$$

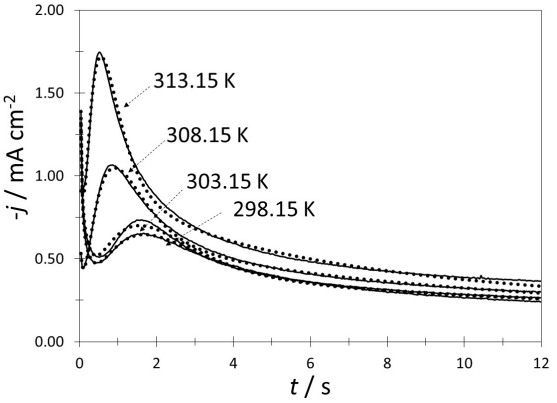

Fig. 9. Comparison between experimental current density transients (straight line) recorded at different temperatures and potentials during the Co electrodeposition on Au(111) with its theoretical transient (OOO) generated by nonlinear fitting of Eq. (7) to the experimental data.

and j_{3D} corresponds to the 3D nucleation and growth under OPD conditions, which is expressed by the following equation (Heerman & Tarallo, 1998):

$$j_{3D-dc} = \frac{nFDC_0}{(\pi Dt)^{1/2}} \bullet \frac{\varnothing}{\theta} \bullet \left\{1-\exp\left[-\alpha_S N_0 (\pi Dt)^{1/2} t^{1/2}\theta\right]\right\} \quad (10)$$

where

$$\varnothing = 1 - \frac{\exp(-At)}{(At)^{\frac{1}{2}}}\int_0^{(At)^{\frac{1}{2}}} \exp\left(\lambda^2\right) d\lambda$$

$$= 1 - \frac{1}{(At)^{\frac{1}{2}}}\left(\frac{0.051314213 + 0.47910725(At)^{\frac{1}{2}}}{1 - 1.2068142(At)^{\frac{1}{2}} + 1.185724(At)}\right) \quad (11)$$

In this model, $j_{3D\text{-}dc}$ represents the current density and $\alpha_S = 2[2V_m DC_0]^{1/2}$, where V_m is the molar volume of the deposit, A is the nucleation rate, and N_0 is the density of active nucleation sites. All other parameters retain their conventional meanings. The analysis of the current density transients obtained in the UPD region is presented in the supplementary material; this analysis shows that the current decay is associated with double-layer charging and two-dimensional instantaneous nucleation processes. Figure 9 compares the experimental current transients with the theoretical curves obtained by nonlinear fitting of the data to equation (7). The model accurately reproduces the behavior of all experimental transients. The kinetic and physical parameters derived from these fits are summarized in Tables 1 and 2. The results show that both the nucleation rate and the density of active sites increase as the applied potential becomes more negative.

The nucleation rate rises systematically with temperature at all potentials, indicating a thermally activated nucleation process.

Table 1. Potential dependence observed for the nucleation rate during cobalt deposition from the Au(111)/0.005 M $CoCl_2$ + 1 M NH_4Cl (pH 9.5) system. The values were obtained from best-fit parameters of the experimental *j-t* plots using Eq. (7).

Potential / V	A (298.15 K) / s^{-1}	A (303.15 K) / s^{-1}	A (308.15 K) / s^{-1}	A (313.15 K) / s^{-1}
-0.96	0.333	0.358	0.482	0.511
-0.95	0.222	0.337	0.295	0.444
-0.94	0.185	0.310	0.290	0.412
-0.93	0.180	0.246	0.282	0.350
-0.92	0.122	0.128	0.154	0.260
-0.91	0.120	0.100	0.189	0.227
-0.90	0.091	0.090	0.139	0.208
-0.89	0.091	0.093	0.103	0.214
-0.88	0.068	0.078	0.096	0.171
-0.87	0.067	0.050	0.063	0.153
-0.86	0.065	0.033	0.064	0.132

Table 2. Potential dependence observed for the number of active nucleation sites during cobalt deposition from the Au(111)/0.005 M $CoCl_2$ + 1 M NH_4Cl (pH 9.5) system. The values were obtained from best-fit parameters of the experimental *j-t* plots using Eq. (7).

Potential / V	$N_0 \times 10^{-7}$ (298.15 K) / cm^{-2}	$N_0 \times 10^{-7}$ (303.15 K) / cm^{-2}	$N_0 \times 10^{-7}$ (308.15 K) / cm^{-2}	$N_0 \times 10^{-7}$ (313.15 K) / cm^{-2}
–0.96	1.327	1.266	1.873	2.495
–0.95	0.96	2.154	2.822	2.590
–0.94	0.862	1.637	1.86	2.268
–0.93	0.869	0.779	1.964	2.339
–0.92	0.638	1.829	2.036	1.956
–0.91	0.356	2.169	2.09	1.891
–0.9	0.649	0.703	0.962	1.726
–0.89	0.876	1.588	1.903	1.522
–0.88	0.134	1.152	1.456	1.545
–0.87	0.52	0.634	0.264	1.394
–0.86	0.153	0.141	0.425	1.130

This effect is particularly pronounced at higher overpotentials, where the increased driving force lowers the energy barrier for stable nucleus formation. Furthermore, N_0 increases exponentially with the applied potential. Although higher temperatures also lead to an increase in N_0, no linear relationship was observed between ln N_0 and $1/T$. This indicates that the number density of active sites is predominantly governed by the applied potential rather than by thermal activation. The average diffusion coefficients were determined to be 1.7×10^{-6}, 1.9×10^{-6}, 2.3×10^{-6} and 3.4×10^{-6} cm^2 s^{-1} for 298.15, 303.15, 308.15 and 313.15 K, respectively. These values are consistent with those reported for similar cobalt plating baths (Mendoza-Huizar & Rios-Reyes, 2013). The increase of the diffusion coefficient with temperature further confirms that mass transport in this system is thermally activated.

Due to the temperature dependence of the nucleation rate constant, it was analyzed using an Arrhenius-type relationship:

$$A = A_0 e^{\left(-\frac{E_a}{RT}\right)} \tag{12}$$

where A_0 is the pre-exponential factor and E_a is the apparent activation energy for nucleation. Linear fits of ln A as a function of $1/T$ were observed for all potentials. The corresponding activation energies derived from the slopes of these plots are summarized in Table 3. These activation energies are consistent with those reported in the literature for nucleation processes (Li & Jun, 2018; Medina-Galván, Quintana-Hernández, Reyes-Valadez, & Fuentes-Cortés, 2020; Tan, He, Gao, Peng, & Dai, 2021; Vazquez-Arenas, Cruz, & Mendoza-Huizar, 2006). Notably, the activation energy decreases as the applied potential is more negative, which suggests that the nucleation process is favored at more negative potential and favored by an increase in temperature, which confirms that cobalt nucleus formation is a thermally activated process, where kinetic contributions dominate over purely thermodynamic effects. Notably, the activation energy decreases as the applied potential becomes more negative. This trend suggests that the nucleation process is energetically favored at higher overpotentials, where the increased driving force lowers the energy barrier for stable

Table 3. Activation energy values of the nucleation rate (E_a) obtained at each potential value.

E / V	E_a/kJ mol^{-1}
–0.96	24.49
–0.95	30.19
–0.94	36.45
–0.93	33.16
–0.92	37.62
–0.91	39.34
–0.90	45.17
–0.89	41.03
–0.88	45.87
–0.87	41.20
–0.86	42.48

nucleus formation. Furthermore, the fact that the rate increases with temperature confirms that cobalt nucleus formation is a thermally activated process, where kinetic contributions dominate over purely thermodynamic effects.

Similarly, the temperature dependence of the diffusion coefficients obtained at different temperatures was analyzed using the Arrhenius equation (Eq. 13).

$$D = D^0 \exp\left(-\frac{\Delta H_D}{RT}\right) \tag{13}$$

In this equation D_0 corresponds to the pre-exponential factor, while ΔH_D represents to the activation energy for the diffusion process. From the plot of ln D versus $1/T$, the linear relationship is expressed as:

$$\ln D = \ln D^0 - \frac{\Delta H_D}{R}\frac{1}{T} \tag{14}$$

The diffusion coefficient shows a clear Arrhenius-type dependence on temperature, with an activation energy of approximately 36 kJ·mol^{-1}. This value is typical for ionic diffusion in aqueous media (Matsumiya, Terazono, & Tokuraku, 2006; Ramos Lora, Mendoza Huizar, Rios-Reyes, & Galán-Vidal, 2014), and is lower than the activation energy determined for nucleation, confirming that cobalt electrodeposition is primarily governed by interfacial kinetic processes rather than being strictly limited by mass transport under the studied temperature range. A direct comparison of the temperature dependencies of A and D shows that, although both nucleation and diffusion are enhanced at higher temperatures, the overall electrodeposition kinetics are dominated by nucleation and growth at the electrode interface.

Additionally, the critical size of the cobalt nucleus (n_c) was evaluated from the relationship between the potential dependence of A and the applied potential using the following equation (Milchev, 1991):

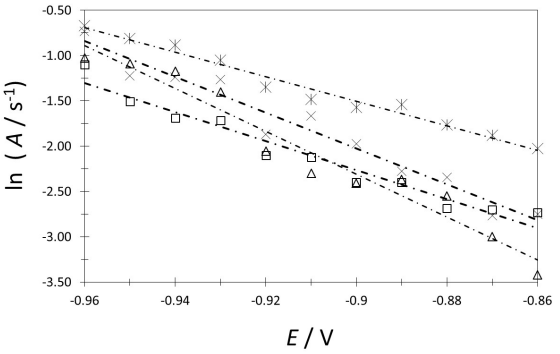

Fig. 10. ln A vs E plot, used to calculate the critical size of the Co nucleus according to Eq. (15). The broken straight line corresponds to the linear fit of the experimental data.

$$n_c = \left(\frac{k_B T}{z e_0}\right)\left(\frac{d \ln A}{dE}\right) - \alpha_{Co} \tag{15}$$

where α_{Co} is the transfer coefficient for cobalt reduction, k is the Boltzmann constant, T is the absolute temperature, z is the valence of the metal ion, and e_0 is the elementary charge. The α_{Co} value calculated in this work is 0.86 at 298.15 K, and similar values were obtained at the other temperatures. The plot of ln A versus the applied potential (E) shows linear behavior (Figure 10). Using Eq. (15), the critical cluster size calculated at the four investigated temperatures was found to be zero (n_c=0). This value implies that a single cobalt atom on an active site constitutes a stable nucleus, indicating that every Co atom deposited on Au(111) is thermodynamically stable (Mendoza-Huizar & Rios-Reyes, 2012). This result is consistent with the high adatom-substrate interaction energy typical of UPD-preceded systems.

Conclusions

Under our experimental conditions, the voltammetric study confirms the coexistence of two cobalt phases on Au(111): a strongly adsorbed underpotential deposition layer stabilized by strong Co–Au interactions, and a three-dimensional bulk-like cobalt deposit formed under overpotential conditions. The OPD process is mainly controlled by 3D progressive nucleation and growth kinetics. Both the nucleation rate (A) and the diffusion coefficient (D) exhibit Arrhenius-type temperature dependence, confirming that cobalt nucleation is a thermally activated process. The increase of A with temperature reflects a reduction in the energy barrier for stable nucleus formation. Furthermore, the activation energy for diffusion (ΔH_D= 36 kJ·mol^{-1}) was found to be lower than the

activation energy for nucleation (Ea). This comparison indicates that the overall electrodeposition kinetics are primarily determined by interfacial nucleation and growth rather than by mass transport limitations within the studied temperature range. Finally, the calculation of a zero critical nucleus size (n_c =0) suggests that a single cobalt atom on an active site is sufficient to form a stable nucleus, highlighting the high affinity of the Au(111) substrate for cobalt adatoms.

Acknowledgements

LHMH and CHRR thankfully acknowledges the computer resources, technical expertise, and support provided by the Laboratorio Nacional de Supercómputo del Sureste de México, CONACYT member of the network of national laboratories through the project No 202501011N. The Guanajuato National Laboratory (CONACyT 123732) is gratefully acknowledged for providing supercomputing resources. LHMH acknowledges the Universidad Autónoma del Estado de Hidalgo for the support granted to carry out this work. LHMH also thanks the SNII for the recognition of his membership and the financial stipend received.

References

Allongue, P., Cagnon, L., Gomes, C., Gündel, A., & Costa, V. (2004). Electrodeposition of Co and Ni / Au (1 1 1) ultrathin layers . Part I : nucleation and growth mechanisms from in situ STM. *Surface Science*, *557*, 41–56. https://doi.org/10.1016/j.susc.2004.03.016

Armstrong, R. D., & Harrison, J. A. (1969). Two-Dimensional Nucleation in Electrocrystallization, *236*(1967), 1967–1970.Armyanov, S. (2000). Crystallographic structure and magnetic properties of electrodeposited cobalt and cobalt alloys. *Electrochimica Acta*, *45*, 3323–3335. https://doi.org/https://doi.org/10.1016/S0013-4686(00)00408-4

Berzins, T., & Delahay, P. (1953). Oscillographic Polarographic Waves for the Reversible Deposition of Metals on Solid Electrodes. *Journal of the American Chemical Society*, *75*(3), 555–559. https://doi.org/10.1021/ja01099a013

Black, A. W., Zhang, W., Noori, Y. J., Reid, G., & Bartlett, P. N. (2023). Temperature effects on the electrodeposition of semiconductors from a weakly coordinating solvent. *Journal of Electroanalytical Chemistry*, *944*, 117638. https://doi.org/10.1016/J.JELECHEM.2023.117638

Bockris, J. O. ., Reddy, A. K. N. ., & Gamboa-Aldeco, M. (2002). *Modern electrochemistry. Volume 2A, Fundamentals of electrodics*. Kluwer Academic.

Bubendorff, J. L., Beaurepaire, E., Mény, C., & Bucher, J. P. (1998). Overpotential driven perpendicular magnetization of electrodeposited ultrathin cobalt films. *Journal of Applied Physics*, *83*(11), 7043–7045. https://doi.org/10.1063/1.367820

Cagnon, L., Gundel, A., Devolder, T., Morrone, A., Chappert, C., Schmidt, J. E., … Allongue, P. (2000). Anion effect in Co/Au(111) electrodeposition: structure and magnetic behavior. *ApSS*, *164*(1), 22–28. https://doi.org/10.1016/S0169-4332(00)00330-5

Chen, Y., Wang, L., Pradel, A., Ribes, M., & Record, M.-C. (2014). A voltammetric study of the underpotential deposition of cobalt and antimony on gold. *Journal of Electroanalytical Chemistry*, *724*, 55–61. https://doi.org/10.1016/J.JELECHEM.2014.03.025

Cortés, A., Lavín, R., Denardin, J. C., Marotti, R. E., Dalchiele, E. A., Valdivia, P., & Gómez, H. (2011). Template Assisted Electrochemical Growth of Cobalt Nanowires : Influence of Deposition Conditions on Structural , Optical and Magnetic Properties. *Journal of Nanoscience and Nanotechnology*, *11*(5), 3899–3910. https://doi.org/10.1166/jnn.2011.3826

Costa, J. M., Portela, D. G., & de Almeida Neto, A. F. (2020). Ni-Co-W Alloys: Influence of Operational Process Conditions on Their Electroplating. *Alloy Materials and Their Allied Applications*, 39–60. https://doi.org/10.1002/9781119654919.ch3

Cruz-Martínez, M. I., Rivera-Hernández, M., Álvarez-Romero, G. A., Nieto-Velázquez, S., & Mendoza-Huizar, L. H. (2021). Electrodeposición de cobalto sobre oro a partir de un baño electrolítico a base de bitartrato. *Pädi Boletín Científico de Ciencias Básicas e Ingenierías Del ICBI*, *9*(Especial2), 145–148. https://doi.org/10.29057/ICBI.V9IESPECIAL2.8011

de Abril, O., Mandler, D., & Unwin, P. R. (2004). Local Cobalt Electrodeposition Using the Scanning Electrochemical Microscope. *Electrochemical and Solid-State Letters*,

7(6), C71. https://doi.org/10.1149/1.1697906

Dean, J, A. (1999). *Handbook of chemistry*. *Soil Science* (Fifteenth). New York: McGraw-Hill, Inc. https://doi.org/10.1016/S0016-0032(40)90947-4

Di, N., Damian, A., Maroun, F., & Allongue, P. (2016). Influence of Potential on the Electrodeposition of Co on Au (111) by In Situ STM and Reflectivity Measurements. *Journal OfThe Electrochemical Society*, *163*(12), 3062–3068. https://doi.org/10.1149/2.0091612jes

Fayette, M., Bertocci, U., & Stafford, G. R. (2016). In Situ Stress Measurements during Cobalt Electrodeposition on (111)-Textured Au. *Journal of The Electrochemical Society*, *163*(5), D146–D153. https://doi.org/10.1149/2.0511605jes

Flis-kabulska, I. (2006). Electrodeposition of cobalt on gold during voltammetric cycling. *Journal of Applied Electrochemistry*, *36*(2), 131–137. https://doi.org/10.1007/s10800-005-9024-8

Gamburg, Y. D., & Zangari, G. (2011). *Theory and Practice of Metal Electrodeposition*. *Theory and Practice of Metal Electrodeposition*. Springer New York. https://doi.org/10.1007/978-1-4419-9669-5

García-Torres, J., Gómez, Æ. E., & Vallés, E. (2009). Modulation of magnetic and structural properties of cobalt thin films by means of electrodeposition. *Journal of Applied Electrochemistry*, *39*, 233–240. https://doi.org/10.1007/s10800-008-9661-9

Graciano, V. P., Bertocci, U., & Stafford, G. R. (2019). In-Situ Stress Measurements during Cobalt Electrodeposition. *Journal of The Electrochemical Society*, *166*(1), D3246. https://doi.org/10.1149/2.0311901JES

Hamulić, D., Milošev, I., & Lützenkirchen-Hecht, D. (2018). The effect of the deposition conditions on the structure, composition and morphology of electrodeposited cobalt materials. *Thin Solid Films*, *667*, 11–20. https://doi.org/10.1016/J.TSF.2018.10.007

Heerman, L., & Tarallo, A. (1998). Electrochemical nucleation on microelectrodes. Theory and experiment for diffusion-controlled growth. *Journal of Electroanalytical Chemistry*, *451*(1–2), 101–109. https://doi.org/10.1016/S0022-0728(98)00101-6

Hsieh, Y., Lai, M., Huang, H., & Sun, I. (2014). Electrochimica Acta Speciation of cobalt-chloride-based ionic liquids and electrodeposition of Co wires. *Electrochimica Acta*, *117*, 217–223. https://doi.org/10.1016/j.electacta.2013.11.120

Kołodziejczyk, K., Miękoś, E., Zieliński, M., Jaksender, M., Szczukocki, D., Czarny, K., & Krawczyk, B. (2018). Influence of constant magnetic field on electrodeposition of metals, alloys, conductive polymers, and organic reactions. *Journal of Solid State Electrochemistry*, *22*, 1629–1647. https://doi.org/10.1007/s10008-017-3875-x

Krause, A., Uhlemann, M., Gebert, A., & Schultz, L. (2004). The effect of magnetic fields on the electrodeposition of cobalt. *Electrochimica Acta*, *49*(24), 4127–4134. https://doi.org/10.1016/j.electacta.2004.04.006

Landa-Castro, M., Sebastián, P., Giannotti, M. I., Serrà, A., & Gómez, E. (2020). Electrodeposition of nanostructured cobalt films from a deep eutectic solvent: Influence of the substrate and deposition potential range. *Electrochimica Acta*, *359*, 136928. https://doi.org/10.1016/j.electacta.2020.136928

Li, Q., & Jun, Y. S. (2018). The apparent activation energy and pre-exponential kinetic factor for heterogeneous calcium carbonate nucleation on quartz. *Communications Chemistry 2018 1:1*, *1*(1), 56-. https://doi.org/10.1038/s42004-018-0056-5

Lin, L. G., Yan, J. W., Wang, Y., Fu, Y. C., & Mao, B. W. (2006). An in situ STM study of cobalt electrodeposition on Au(111) in BMIBF4 ionic liquid. *Journal of Experimental Nanoscience*, *1*(3), 269–278. https://doi.org/10.1080/17458080601009643

Lützenkirchen-Hecht, D., Hamulić, D., Wagner, R., & Milošev, I. (2020). EXAFS investigations of cobalt electrodeposition. *Radiation Physics and Chemistry*, *175*, 108113. https://doi.org/10.1016/J.RADPHYSCHEM.2018.12.033

Marsh, D. A., Yan, W., Liu, Y., Hemminger, J. C., Penner, R. M., & Borovik, A. S. (2013). Water oxidation using a cobalt monolayer prepared by underpotential deposition. *Langmuir*, *29*(47), 14728–14732. https://doi.org/10.1021/la403038e

Martell, A. E., & Smith, R. M. (1976). *Critical Stability Constants Volume 4* (Vol. 4). Texas: Springer.Matsumiya, M., Terazono, M., & Tokuraku, K. (2006). Temperature dependence of kinetics and diffusion coefficients for ferrocene/ferricenium in ammonium-imide ionic liquids. *Electrochimica Acta*, *51*(7), 1178–1183. https://doi.org/10.1016/J.ELECTACTA.2005.06.006

Mech, K., Zabiński, P., Kowalik, R., & Fitzner, K. (2012). EQCM, SEC and voltammetric study of kinetics and mechanism of hexaamminecobalt(III) electro-reduction onto gold electrode. *Electrochimica Acta*, *81*, 254–259. https://doi.org/10.1016/j.electacta.2012.07.067

Medina-Galván, X. M., Quintana-Hernández, P. A., Reyes-Valadez, J. N., & Fuentes-Cortés, L. F. (2020). acetilsalicílico e…Determination of kinetic parameters of nucleation and growth of acetylsalicylic acid crystals in ethanol. *Revista Mexicana de Ingeniera Quimica*, *19*(1), 445–456. https://doi.org/10.24275/rmiq/Cat1574

Mendoza-Huizar, L. H., & Rios-Reyes, C. H. (2012). Cobalt electrodeposition on polycrystalline palladium. Influence of temperature on kinetic parameters. *Journal of Solid State Electrochemistry*, *16*(9). https://doi.org/10.1007/s10008-012-1722-7

Mendoza-Huizar, L. H., & Rios-Reyes, C. H. (2013). Cobalt electrodeposition onto polycrystalline gold from ammoniacal solutions. *Central European Journal of Chemistry*, *11*(8), 1381–1392. https://doi.org/10.2478/s11532-013-0269-5

Mendoza-Huizar, L. H., Robles, J., & Palomar-Pardave, M. (2005). Theoretical and experimental study of cobalt nucleation and growth onto gold substrate with different crystallinity. *Journal of the Electrochemical Society*, *152*(5), C265-c271. https://doi.org/10.1149/1.1873472

Mendoza-Huizar, L. H., Robles, J., & Palomar-Pardavé, M. (2003). Nucleation and growth of cobalt onto different substrates - Part II. The upd-opd transition onto a gold electrode. *Journal of Electroanalytical Chemistry*, *545*(SUPPL.), 39–45. https://doi.org/10.1016/S0022-0728(03)00087-1

Mendoza-Huizar, L., Robles, J., & Palomar-Pardavé, M. (2002). Nucleation and growth of cobalt onto different substrates - Part I. Underpotential deposition onto a gold electrode. *Journal of Electroanalytical Chemistry*, *521*(1–2), 95–106. https://doi.org/10.1016/S0022-0728(02)00659-9

Mendoza-Huizar, Luis, & Rios-Reyes, C. (2013). Cobalt electrodeposition onto polycrystalline gold from ammoniacal solutions. *Open Chemistry*, *11*(8), 1381–1392. https://doi.org/10.2478/s11532-013-0269-5

Milchev, A. (1991). Electrochemical phase formation on a foreign substrate — basic theoretical concepts and some experimental results Electrochemical phase formation on a foreign substrate-basic theoretical concepts and some experimental results. *Contemporary Physics*, *32*(5), 321–332. https://doi.org/10.1080/00107519108223705

Montes-Rojas, A., Torres-Rodríguez, L. M., & Nieto-Delgado, C. (2007). Electromicrogravimetric study of underpotential deposition of Co on textured gold electrode in ammonia medium. *New Journal of Chemistry*, *31*(10), 1769–1776. https://doi.org/10.1039/B704891B

Motobayashi, K., Nakagawa, H., Shibamura, Y., & Ikeda, K. (2023). Origin of Temperature-Dependent Overpotential of Co Electrodeposition in an Ionic Liquid. *The Journal of Physical Chemistry C*, *128*(2), 819–826. https://doi.org/10.1021/ACS.JPCC.3C07750

Nemtoi, G., Chiriac, H., Dragos, O., Apostu, M.-O., & Lutic, D. (2009). The Voltammetric Characterization of the Electrodeposition of Cobalt , Nickel and Iron on Gold Disk Electrode. *Acta Chemica Iasi*, *17*, 151–168. https://doi.org/https://www.chem.uaic.ro/files/file/acta-chemica/2009/no-2-2009/aci_vol_17_no_2_2009_article-3.pdf

Paunovic, M., & Schlesinger, M. (2006). *Fundamentals of Electrochemical Deposition* (2nd Edition). Hoboken, N.J.: John Wiley & Sons.Puigdomenech, I. (2004). HYDRA (Hydrochemical Equilibrium- Constant Database) and MEDUSA (Make Equilibrium Diagrams Using Sophisticated Algorithms) Programs.

Stockholm: KTH Royal Institute of Technology. https://doi.org/https://www.kth.se/polopoly_fs/1.369371.1600688803!/Eq-Calcs_32.zip

Ramos Lora, N., Mendoza Huizar, L. H., Rios-Reyes, C. H., & Galán-Vidal, C. A. (2014). *Influence*

of the temperature on the diffusion coefficient value during the cobalt electrodeposition on different substrates. *Advanced Materials Research* (Vol. 976). https://doi.org/10.4028/www.scientific.net/AMR.976.144

Rojas-Hernández, A., Ramírez, M. T., Ibáñez, J. G., & González, I. (1991). Construction of Multicomponent Pourbaix Diagrams Using Generalized Species. *Journal of The Electrochemical Society*, *138*(2), 365–371. https://doi.org/10.1149/1.2085590

Scharifker, B., & Hills, G. (1983). Theoretical and experimental studies of multiple nucleation. *Electrochimica Acta*, *28*(7), 879–889. https://doi.org/10.1016/0013-4686(83)85163-9

Szmaja, W., Kozłowski, W., Polański, K., Balcerski, J., Cichomski, M., Grobelny, J., Mięko ś, E. (2012). Study of the morphological and magnetic structures of nanocrystalline cobalt films obtained by electrodeposition. *Materials Chemistry and Physics*, *132*(2–3), 1060–1064. https://doi.org/10.1016/J.MATCHEMPHYS.2011.12.065

Tan, W., He, H., Gao, Y., Peng, Y., & Dai, X. (2021). Nucleation and growth mechanisms of an electrodeposited Ni–Se–Cu coating on nickel foam. *Journal of Colloid and Interface Science*, *600*, 492–502. https://doi.org/10.1016/J.JCIS.2021.05.002

Vazquez-Arenas, J., Cruz, R., & Mendoza-Huizar, L. H. (2006). The role of temperature in copper electrocrystallization in ammonia-chloride solutions. *Electrochimica Acta*, *52*(3), 892–903. https://doi.org/10.1016/j.electacta.2006.06.022

Wei, G., Ge, H., Wu, Q., Yu, Y., Wang, X., & Chen, C. (2009). Co – Pt – W thin films electrodeposited from sulphate – gluconate baths. *Materials Chemistry and Physics 118*, *118*, 57–62. https://doi.org/10.1016/j.matchemphys.2009.07.003

Wu, H., Zei, M., & Yau, S. (2010). Reflection high-energy electron diffraction characterization of cobalt clusters electrodeposited on a Au(100) electrode. *Journal of Physical Chemistry C*, *114*(47), 20062–20067. https://doi.org/10.1021/jp1065924